APPLIED SCIENCES AND ENGINEERING

Wirelessly powered deformable electronic stent for noninvasive electrical stimulation of lower esophageal sphincter

Chong Zhang[1]†, Chengfeng Pan[2,3]†, Kai Fung Chan[1,4,5]*, Jinyang Gao[2], Zhengxin Yang[2], Kevin Kai Chung Leung[5], Dongdong Jin[2], Yuqiong Wang[2], Neng Xia[2], Zhipeng Ning[2], Xin Wang[2], Shuai Jiang[1], Zifeng Zhang[2], Qinglong Wang[2], Bo Hao[2], Philip Wai Yan Chiu[4,5,6]*, Li Zhang[1,2,5,6]*

Electrical stimulation is a promising method to modulate gastrointestinal disorders. However, conventional stimulators need invasive implantation and removal surgeries associated with risks of infection and secondary injuries. Here, we report a battery-free and deformable electronic esophageal stent for wireless stimulation of the lower esophageal sphincter in a noninvasive fashion. The stent consists of an elastic receiver antenna infilled with liquid metal (eutectic gallium-indium), a superelastic nitinol stent skeleton, and a stretchable pulse generator that jointly enables 150% axial elongation and 50% radial compression for transoral delivery through the narrow esophagus. The compliant stent adaptive to the dynamic environment of the esophagus can wirelessly harvest energy through deep tissue. Continuous electrical stimulations delivered by the stent in vivo using pig models significantly increase the pressure of the lower esophageal sphincter. The electronic stent provides a noninvasive platform for bioelectronic therapies in the gastrointestinal tract without the need for open surgery.

INTRODUCTION

Gastroesophageal reflux disease (GERD) is a common gastrointestinal (GI) disorder that shows a worldwide prevalence of around 8 to 33% (*1*, *2*). It is characterized by gastric acid content abnormally flowing back into the esophagus, mainly because of the transient relaxation of the lower esophagus sphincter (LES) (*3*, *4*). Long-term exposure to gastric acid will irritate the esophagus, inducing symptoms of chest pain, chronic inflammation, and ulceration (*5*), and may lead to severe complications including esophageal strictures, Barrett's esophagus (*6*), and even esophagus cancer (*7*).

Medication therapy, such as proton pump inhibitors, is primarily used in clinics to mitigate acid-induced symptoms by inhibiting gastric acid secretion. However, a large group of GERD patients still suffer from recurrent symptoms due to poor drug adherence (*8*, *9*) and will seek surgical interventions as an alternative. Fundoplication is a typical surgical procedure to treat GERD where the fundus is folded and sewn around the LES to passively reinforce its barrier function (*10*). Another similar strategy without changing the anatomical structure of the gastroesophageal junction is magnetic sphincter augmentation, which uses a ring of magnetic beads to tighten LES (*11*). Despite the effective control of symptoms, these passive and unnatural augmentations of LES may lead to undesired side effects (e.g., difficulty in swallowing, abdominal bloating, and increased flatulence) and potential severe risks associated with laparoscopic surgeries (e.g., inflammation, abdominal pain, and bleeding) (*12*–*14*).

Electrical stimulation therapy (EST) is a promising effective method to treat GERD, which may address the need of a large group of GERD patients who suffer from inadequate symptom control of medications (*15*) and worry about the potential risks of anti-reflux surgeries (fundoplication) or implanting LES augmentation devices (*16*–*17*). Other than passive LES augmentation, EST actively enhances LES muscles to increase the closure pressure of LES without affecting the normal relaxation of LES as the anatomical structure of the gastroesophageal junction is preserved (*18*). Previous clinical trials suggest that long-term intermittent electrical stimulation can restore the normal barrier functions of LES and thus eliminate GERD from the root (*19*, *20*). However, conventional implantable EST devices for GERD treatment (e.g., EndoStim) share the same limitations and potential risks associated with the invasive surgeries requirement: to implant the pulse generator in the abdominal cavity, to fix the electrodes to the muscular layer of the esophagus, and to remove the implanted EST system after the completion of therapy (*21*). Besides, conventional implantable EST devices may cause unexpected events including accidental stimulation to abdominal muscles or diaphragm, migration of implanted stimulator in subcutaneous space, and electrodes dislodgement and even electrode perforation into the esophagus, which will require additional surgeries for repositioning. (*22*). The heavy surgical burden (i.e., invasive surgery) and concomitant potential risks prevent the widespread implementation of implantable EST systems (see comparisons of GERD therapies in table S1). Overall, with the increasing prevalence of GERD patients worldwide, there is a strong demand for developing an EST system with less invasiveness to minimize open surgery–induced risks and increase the acceptance of EST for GERD patients (*23*).

[1]Department of Biomedical Engineering, The Chinese University of Hong Kong, Shatin, New Territories, Hong Kong SAR, China. [2]Department of Mechanical and Automation Engineering, The Chinese University of Hong Kong, Shatin, New Territories, Hong Kong SAR, China. [3]The State Key Laboratory of Fluid Power and Mechatronic Systems, College of Mechanical Engineering, Zhejiang University, Hangzhou 310027, P. R. China. [4]Chow Yuk Ho Technology Center for Innovative Medicine, The Chinese University of Hong Kong, Shatin, New Territories, Hong Kong SAR, China. [5]Multi-Scale Medical Robotics Center, Hong Kong Science Park, Shatin, New Territories, Hong Kong SAR, China. [6]Department of Surgery, The Chinese University of Hong Kong, Shatin, New Territories, Hong Kong SAR, China.
†These authors contributed equally to this work.
*Corresponding author. Email: lizhang@mae.cuhk.edu.hk (L.Z.); philipchiu@surgery.cuhk.edu.hk (P.W.Y.C.); kaifungchan@cuhk.edu.hk (K.F.C.)

The GI tract offers the opportunity to deliver biomedical devices in a noninvasive way (*24*–*27*). However, designing bioelectronics that operate locally and continuously within the tubular organs of the GI tract, such as the esophagus, remains challenging mainly due to the anatomical structure of these organs. Specifically, the esophagus is a long narrow muscular tube located in deep tissue. First, the narrow space of the esophagus precludes the bulky batteries used in conventional stimulators. Despite tremendous efforts in wireless power transfer technology (table S2) (*28*–*32*), it is still challenging to power bioelectronics in deep tissue (>10 cm), especially within large animal models. Second, the limited space also requires a transformable structure for the transoral delivery procedure while retaining itself within the esophagus during continuous operation without affecting swallowing function. Third, the esophagus generates peristalsis movements and is protected by the mucosa layer. A specific tissue-device interface is required for effective electrical stimulations across the dielectric of the mucosa tissue.

To fulfill the unmet clinical need and address the technical challenges, we present a wireless, battery-free, deformable electronic stent (E-Stent) capable of performing endoscopic delivery through the esophagus from the mouth for the wireless stimulation of LES (Fig. 1A). E-Stent comprises a nitinol esophageal stent as the mechanical support, an elastic coil infilled with liquid metal (LM) [eutectic gallium-indium (EGaIn)] for wireless power transfer, and a stretchable circuit integrated with microneedles (MNs) for reliable electrical stimulations across the mucosa. We characterize the electrical performance of the elastic coil and demonstrate the stable pulse generation of the stretchable circuit under deformation. We then show the transoral delivery of deformable E-Stent by a customized delivery catheter compatible with operation under x-ray fluoroscopy. Moreover, the efficacy and safety of electrical stimulation delivered by the wireless-powered E-Stent are validated in adult pig models. These preclinical results open promising opportunities for in situ bioelectronic therapies with minimal invasiveness in the GI tract.

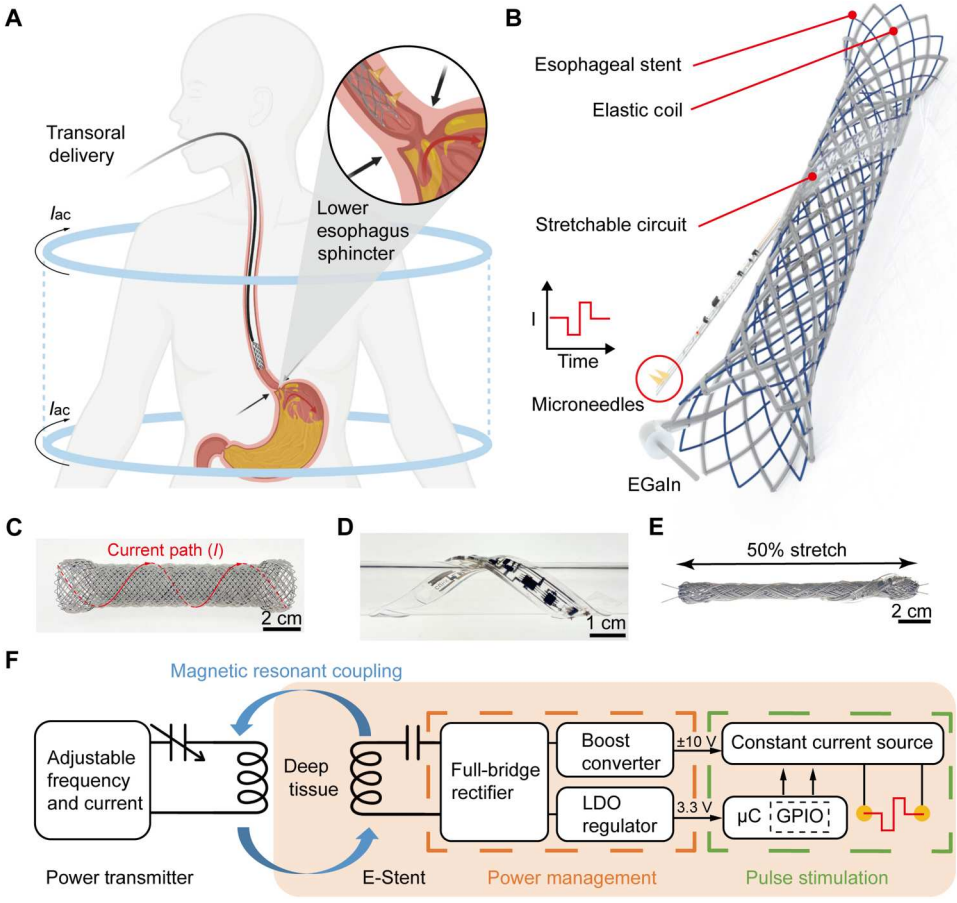

Fig. 1. Overview of the wirelessly powered deformable electronic stent. (**A**) Schematic illustration of E-Stent delivered through the esophagus to the LES for noninvasive electrical stimulation. E-Stent is powered by an external power transmitter. Microneedles (MNs) deliver electrical stimulation across the mucosa, leading to increased pressure of LES (inset). (**B**) Schematic illustration of E-Stent, comprising an elastic coil, an esophageal stent, and a stretchable circuit integrated with MNs. (**C** to **E**) Photographs of the elastic coil braided along the esophageal stent (C), the stretchable circuit wrapped around a transparent acrylic tube (D), and a stretched E-Stent (E). (**F**) Function diagram showing an external power transmitter module and E-Stent including a power management module and a pulse stimulation module for biphasic constant current stimulations. LDO, low dropout. GPIO, general-purpose input/output.

RESULTS

System overview and design of E-Stent

Figure 1A summarizes the working principle and key features of E-Stent. The soft form factor of E-Stent enables large deformations including longitudinal elongation and radial compression that facilitate transoral delivery and avoid the potential risks associated with open surgeries. E-Stent is wirelessly powered by an external power transmitter (fig. S1 and movie S1) based on the principle of magnetic resonant coupling that eliminates the need for any rigid and bulky batteries (*33*). This E-Stent delivers constant biphasic current stimulations to the muscle of LES through a pair of integrated MN electrodes, which can penetrate across the mucosa layer without perforation. Continuous stimuli would significantly increase the pressure of LES and thus reduce gastric acid reflux (Fig. 1A, inset).

Figure 1B illustrates the components of E-Stent. Specifically, E-Stent consists of a commercial nitinol esophageal stent (MicroTech) as the mechanical skeleton, an elastic coil as the receiver antenna to harvest energy by wireless power transfer even under the compression of the esophagus, and a stretchable circuit that can generate precisely timed pulses in the dynamic environment of the esophagus. As shown in Fig. 1C, the elastic coil is braided along the stent skeleton by a single silicone tube (inner diameter of 0.3 mm and outer diameter of 0.8 mm) infilled with EGaIn, LM with low melting point (15.4°C), and metallic electrical conductivity (3.4×10^6 Sm^{-1}) (*34*–*38*). Because of its liquid nature under body temperature, the LM core in the silicone tube is compliant with deformations. The parallelogram mesh allows E-Stent to elongate along the axial direction and shrink in the radial direction when E-Stent is stretched or compressed. Figure 1D shows a photograph of the stretchable circuit wrapped around a transparent acrylic tube indicating its deformability enabled by a laser-assisted maskless fabrication method (see Materials and Methods and fig. S2) (*39*). Metallic compounds of Au and EGaIn are used as the conductive traces to connect electronic components between soft polydimethylsiloxane (PDMS) substrate and encapsulation. The stretchable circuit is integrated with E-Stent along the helical skeleton that minimizes the strain mismatch between the metal skeleton and soft electronics during deformations. The intrinsically stretchable electronics and the transformable structure of the stent skeleton jointly enable E-Stent to undergo extreme deformations (up to 150% elongation in length and 50% shrinkage in diameter) (Fig. 1E). The excellent deformability allows E-Stent to be delivered by a customized catheter through the esophagus from the mouth, which provides a noninvasive accessible route to the LES. Figure S3 shows photographs of the integrated E-Stent. The hollow structure of E-Stent enables the elastic coil to harvest energy without affecting the food passage. The deformable structure and the soft materials of E-Stent are compatible with the complex environment of the esophagus, while the self-expandable nitinol stent skeleton provides intimate and safe contact with esophageal tissue.

Figure 1F illustrates the electrical signal flow of E-Stent (see fig. S4 for details of the circuit design). The external power transmitter is driven by constant currents. The double-solenoid configuration generates a relatively uniform alternative magnetic field along the axial direction of the cylindrical workspace (fig. S5, A to C). The elastic coil serves as the receiver antenna to harvest energy inside the esophagus. The stretchable circuit comprises two main modules of power management and electrical pulse generator. In the power management module, the received alternating current (AC) is converted into direct current (DC) by a full-bridge rectifier. Then, the boost converter elevates the voltage to 10 V and provides a dual-rail power supply to the constant current source. Meanwhile, a low dropout regulator further smooths the received voltage and offers stable 3.3 V to a microcontroller (MCU), which generates two-channel voltage pulses that control the frequency and pulse width of stimulation signals. The constant current source (*40*) converts two-channel monophasic pulse signals into biphasic constant current stimulation pulses in response to variable tissue resistances. This stretchable circuit generates stable pulse signals regardless of the variable output voltage of the elastic coil. The small packages of these components and intrinsic conductive traces realize a highly integrated circuit with 31 components in a miniaturized size (10 mm in width, 75 mm in length, and 1.5 mm in thickness) (fig. S4B).

Elastic coil for wireless power transfer in the esophagus

To provide quantitative guidelines for the electrical performance of the elastic coil, we use an analytical expression to explain and estimate its open-circuit voltage (V_{oc}) based on an enclosed area-dependent model (see details of explanation in text S1 and fig. S6). In general, the open-circuit voltage induced by the elastic coil depends on the change ratio of the magnetic flux across the elastic coil, which is primarily associated with the total area enclosed by the elastic coil. Figure 2A shows the open-circuit voltage of the elastic coils with different sizes in terms of diameter and length when the driving current is 2 A. We have to carefully tune the working frequency of transmitting circuit at 220 kHz to match the resonant frequency of transmitting coils for the high energy efficiency due to the sharp bandwidth of transmitting coils (fig. S5D). A larger size encloses more area, resulting in a higher V_{oc}. We measured V_{oc} of a series of elastic coils with different sizes that fit well with the theoretical values (fig. S7). Considering that the diameter of the human esophagus is approximately 2 cm (*41*), we choose the stent with a diameter of 2 cm and a length of 12 cm for the prototype fabrication of E-Stent. Its theoretical open-circuit voltage is 10.64 V, which is sufficient to drive the circuit for electrical stimulations.

To further investigate the output performance of the elastic coil under the complex condition in the esophagus, we apply angular misalignment and radial compression to the elastic coil at benchtop (see details in Materials and Methods) to simulate the misalignment between E-Stent (i.e., receiver) and transmitter, and the potential compression of the esophagus in practical in vivo applications. Figure 2B shows that the open-circuit voltage maintains above 80% of the maximum voltage (10.76 ± 0.18 V at 30°) and the elastic coil still harvests 7.56 ± 0.59 mW when the angle misaligns up to 30°. The angular stability is mainly attributed to the uniform magnetic field generated by the power transmitter (fig. S5, B and C). The good tolerance to angular misalignment would be beneficial for potential applications where E-Stent may misalign from the axis of the transmitter coil due to the anatomical structure of the esophagus or body movement. The electrical performance of the elastic coil also depends on the deformations. When the elastic coil is compressed to 70% of its original diameter (from 20 to 14 mm), the open-circuit voltage drops approximately 50% from 10.66 ± 1 V to 5.46 ± 0.4 V and the harvested power decreases around 25% from 11.43 ± 2.11 mW to 3 ± 0.45 mW as expected because the enclosed area is reduced by half (Fig. 2C). We also use the modified

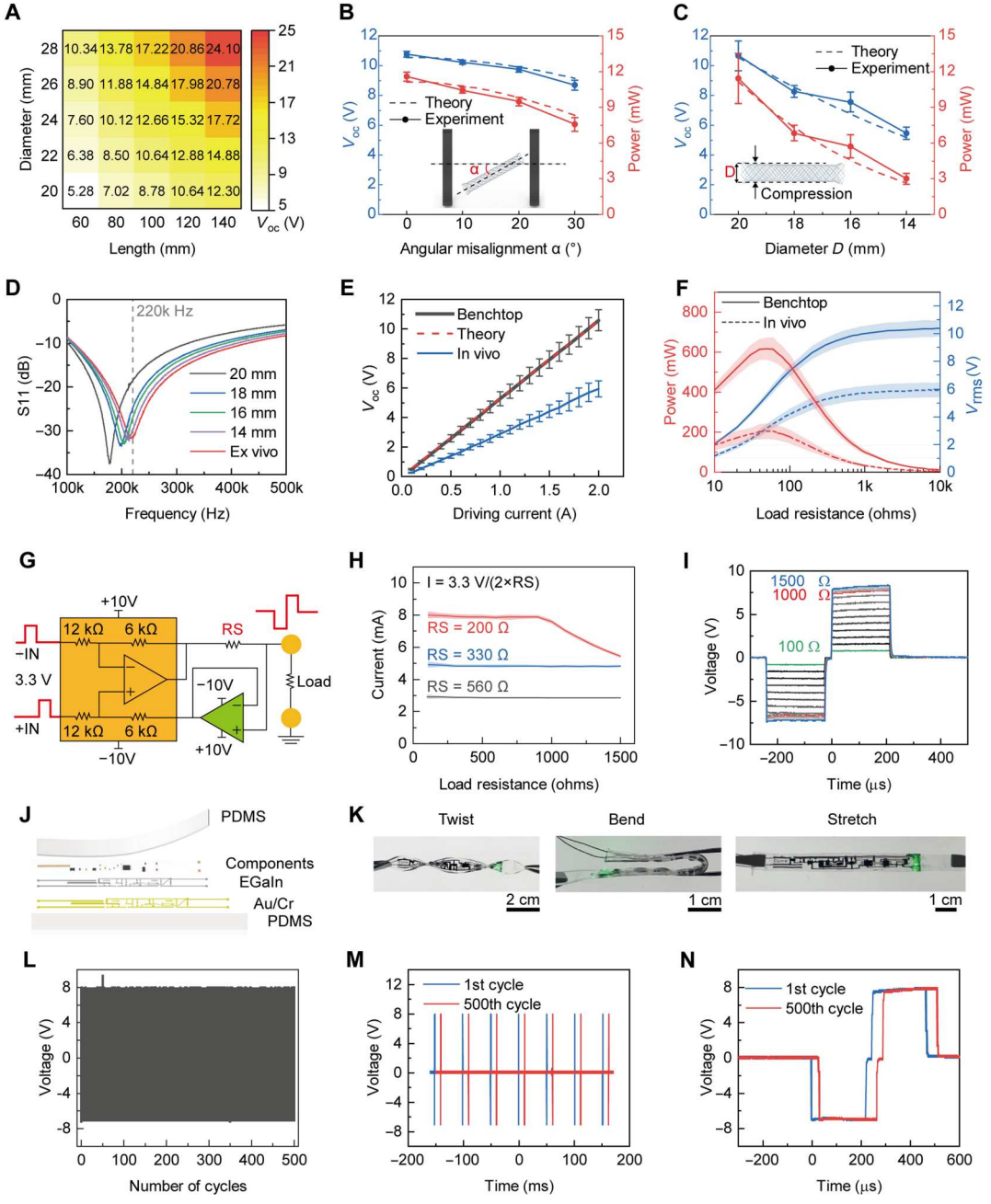

Fig. 2. Electrical performance characterization. (**A**) Theoretical open-circuit voltage of the elastic coil as a function of the length and diameter of E-Stent. (**B** and **C**) Theoretical and experimental values of the open-circuit voltage and related power at 10,000-ohm load resistance as a function of the angular misalignment (B) and diameter (C) of the compressed elastic coil. Mean ± SD for $N = 5$ samples. (**D**) S11 values of the elastic coils with different compressions and inside ex vivo esophagus. (**E**) Theoretical and experimental values of the open-circuit voltage as a function of the driving current. Mean ± SD for $N = 5$ samples. (**F**) Relationship of the output voltage and related power with load resistances. Mean ± SD for $N = 5$ samples. (**G**) Circuit diagram of the voltage-controlled constant current source. (**H**) Constant current output with different current limiting resistor RS as a function of load resistances. (**I**) Biphasic pulse signals with RS of 200 ohms as a function of load resistances. (**J**) Explosive view of the stretchable circuit. (**K**) Photographs of the stretchable circuit under twisting, bending, and stretching. (**L** to **N**) Pulse signals with constant amplitudes (L), frequency (M), and pulse width (N) during 500-times cyclical bending, respectively.

analytical expression to predict the electrical performance under angular misalignment and radial compression (see details in text S2). All experimental results show good agreement with the theoretical value of the enclosed area-dependent model. Unlike angular misalignment that affects the cross-section area enclosed by the elastic coil, compression directly changes its geometry configuration and hence its inductance (fig. S8A). To investigate the effect of compression on resonant frequency, we first placed the elastic coil inside a fresh esophagus of pig to simulate the natural compression of the esophagus and matched the antenna to an operation frequency of 220 kHz. We then measured S11 signals of the elastic coil under different compressions, and the results are presented in Fig. 2D. While resonant frequency shifts to higher frequency under compressions, all S11 values at 220 kHz are below −10 dB, indicating that reflected power is less than 10%. For a transformable antenna, matching it to the operational frequency at its working status would minimize its return loss. We assume that decreased enclosed area is the major factor accounting for the voltage drop during compressions.

We further measure the electrical performance of the chosen elastic coil on the benchtop and in vivo in a pig's esophagus (see Materials and Methods). For an elastic coil with a typical geometry configuration, the open-circuit voltage also depends on the magnetic field intensity, which increases linearly with the driving current both at benchtop and in vivo (Fig. 2E). Figure S9 shows the linear relationship of input voltage with driving current, which derives the input power as 20.62 W with the driving current of 2 A. However, the elastic coil provides a smaller V_{oc} in vivo than benchtop experiments. The decrease in inductance suggests that compression of E-Stent in the esophagus due to muscular contraction is the major factor accounting for the in vivo voltage drop rather than angular misalignment and tissue attenuation (fig. S7B). The electrical behaviors with increasing loads are shown in Fig. 2F. As the load resistance approaches 10,000 ohms, the output voltages saturate to open-circuit voltages of 10.59 ± 0.72 V at benchtop and 5.94 ± 0.53 V in vivo. Moreover, power reaches the peak when the load resistance reaches equilibrium with the elastic coil. When the input voltage is 5 V, the average current consumption of the stretchable circuit is 5.22 mA, suggesting an equivalent load resistance around 1000 ohms. Although the available power drops heavily as the load resistance increases, the elastic coil still harvests approximately 100.53 ± 10.98 mW at benchtop and 32.96 ± 6.23 mW in vivo with a load resistance of 1k ohms. In addition, the peak power consumption of the stretchable circuit is 83.9 mW and the average power is 26. 1 mW (fig. S10). These results indicate that the wireless-powered elastic coil can harvest sufficient electrical energy inside the esophagus to power the stretchable circuit for electrical stimulation with a large capacitor of 10 μF.

Stretchable circuit for stable operation under large deformations

To provide reliable electrical stimulation regardless of variable input voltage, we implement a voltage-controlled current source, including a difference amplifier and an operational amplifier (Fig. 2G). It generates biphasic constant current pulse signals. The frequency and pulse width are controlled by two independent 3.3-V pulse signals generated by the MCU (fig. S11). The amplitudes can be adjusted by the current limiting resistor RS (Fig. 2H). The current source can generate 3- to 10-mA constant current stimulations. In addition, the current driving capability is limited by the supply voltage from the boost converter. When powered by ±10 V, the current source can generate 8-mA biphasic constant current stimulations with load resistance ranges from 100 to 800 ohms (Fig. 2I), which suggests that when load resistance satisfy $V = I^* R_{load} + 3.3\ V/2 < 10\ V$, constant current stimulation is guaranteed. Overall, the circuit provides similar stimulations by a clinically validated stimulator (EndoStim). Previous studies have shown that parameters of the pulse signals play a vital role in effective stimulations of LES (*42*, *43*). We programmed the pulse generator to produce pulses with a frequency of 20 Hz and a pulse width of 215 μs similar to EndoStim, and the stimulation current is set as 8 mA.

To offer good compliance to the dynamic environment of the esophagus, we fabricate a stretchable circuit that robustly generates reliable electrical pulses even under extreme deformations. Figure 2J shows the explosive view of the stretchable circuit, including a biphasic layer formed by EGaIn and Au/Cr intermetallic compounds, electrical components, and PDMS substrate and encapsulation. The EGaIn-based biphasic circuit traces provide not only good electrical conductivity (*44*) but also a stable interface between rigid components and soft substrate (fig. S12, A and B). Large surface tension of EGaIn provides additional forces to ensure that components stably adhere to the substrate (fig. S12, C and D). Figure 2K demonstrates that the stretchable circuit keeps electrically stable during twisting, bending, and stretching. We also perform mechanical tests to study the failure point in the stretching and twisting. Figure S13 shows that the stretchable circuit fails at an average of 41.33% stretching and 1080° (three turns) twisting, suggesting excellent mechanical properties. To further investigate the potential long-term applications of E-Stent in dynamic in vivo environment, we performed cyclic tests of stretchable circuits under mechanical deformation of bending, twisting, and stretching. Figure 2 (L to N) and fig. S14 present stable amplitudes, frequency, and pulse width with cyclic bending (80° bending angle), twisting (360° twisting angle), and stretching (10% strain), respectively. Figure S15 shows negligible change in internal resistance and inductance of the elastic coils with cyclic stretching (10% strain) over 1000 times. These results indicate robust electromechanical performance of the stretchable circuits and the elastic coil independently.

We then integrate the stretchable circuit with the elastic coil and test its performance during stretching, bending, and compression (movie S2). E-Stent demonstrates constant light intensity and frequency during stretching. The constant light intensity and frequency of the integrated light-emitting diode (LED) indicator show robust performance under mechanical deformations. Overall, the circuit design and intrinsic soft materials enable E-Stent to deliver programmable and reliable electrical stimulation signals during deformations, which ensures its robust operation in the dynamic environment of the esophagus.

Deformable E-Stent for transoral delivery

We make a customized delivery catheter to assist the noninvasive delivery of E-Stent from mouth to esophagus. As shown in fig. S16, the customized catheter composes of a commercial balloon catheter (Changmei Medtech), a three-dimensional (3D)–printed soft tip, a flexible shell, and a rigid block ring. The soft material and transformable structure allow E-Stent to be compressed inside a flexible shell tube with a diameter of 12 mm, comparable to a standard endoscope. EGaIn in the elastic coil is the radio-

opaque material that facilitates the operation under fluoroscopy in practical applications. To visualize the delivery procedure of E-Stent, we perform an in vivo delivery in a pig's esophagus under fluoroscopy (Fig. 3A) with the following processes: (i) The customized delivery catheter is inserted into the esophagus (Fig. 3A, top). The soft tip and flexible tube provide soft contact with esophageal tissue and allow smooth delivery without injury (fig. S17). (ii) After E-Stent is delivered above the gastroesophageal junction, the flexible tube is pulled out to release the self-expandable E-Stent and the blocking ring avoids the movement of E-Stent due to friction (Fig. 3A, middle). (iii) The balloon catheter is then inflated to insert the MNs across the mucosa layer after E-Stent is fully released (Fig. 3A, bottom). Figure 3B and movie S3 show the endoscopic view of E-Stent tightly in contact with the esophagus and leaving LES closed. We also measured LES pressure before and after E-Stent deployment (see Materials and Methods). Paired *t* test shows no significant pressure change, suggesting that E-Stent delivery does not affect the closure of LES (Fig. 3C). The open channel allows an endoscope to pass through, which implies that the deformable E-Stent would not inhibit the passage of food through the esophagus. The esophagus also provides a noninvasive way to remove E-Stent as shown in movie S5. Endoscopic view in movie S6 shows a careful inspection of esophagus, and esophagus histology shows that no visible injuries were observed after E-Stent deployment and retrieval (fig. S17). This strategy avoids additional open surgery to remove the conventional pulse generators.

To further validate the MN electrodes delivering effective stimulations across the mucosa layer to the muscle, we characterize the MNs in vivo in four pigs. Figure S18 shows a pair of MN electrodes (1 mm in length; see fig. S19 for details of its geometry configuration) that are integrated with the stretchable circuit and mounted on the outer layer of E-Stent. The stent skeleton made of shape memory nitinol provides radial force to push MNs against the esophagus wall (fig. S20). The histology result further confirms that the MN penetrates across the mucosa layer without perforation (Fig. 3D). To demonstrate the benefit of MNs, we performed in vivo studies using E-Stent with and without MNs for electrical stimulation (see details in Materials and Methods). The profiles of LES pressure for 20 min were recorded during electrical stimulation by E-Stents with and without MNs, respectively. Paired *t* test shows a significant change of average pressure between the devices with and without MNs, indicating that MNs are providing a benefit for the electrical stimulation through mucosa (Fig. 3E).

Considering acid reflux, we coat MNs with a 200-nm Au layer (see Materials and Methods) to avoid acid corrosion. We immerse MNs with and without Au coatings in simulated gastric fluid (SGF; pH 1.5) for 1 week to study electrode stability. Scanning electron microscopy (SEM) images indicate no obvious corrosion in MNs with Au coatings (Fig. 3F). Electrochemical study shows that MNs with Au coating have minimal impedance change at 20 Hz, while the impedance of groups without coating drops from 10^5 to 10^4 ohms. We also immerse the elastic coil and the stretchable circuit in SGF for 4 weeks to examine their stability in acid environment. Figure S21 shows minimal resistance and inductance change of the elastic coil, and the stretchable circuit can still generate precise timed pulses. Overall, these results suggest potential long-term applications of E-Stent in an acid environment.

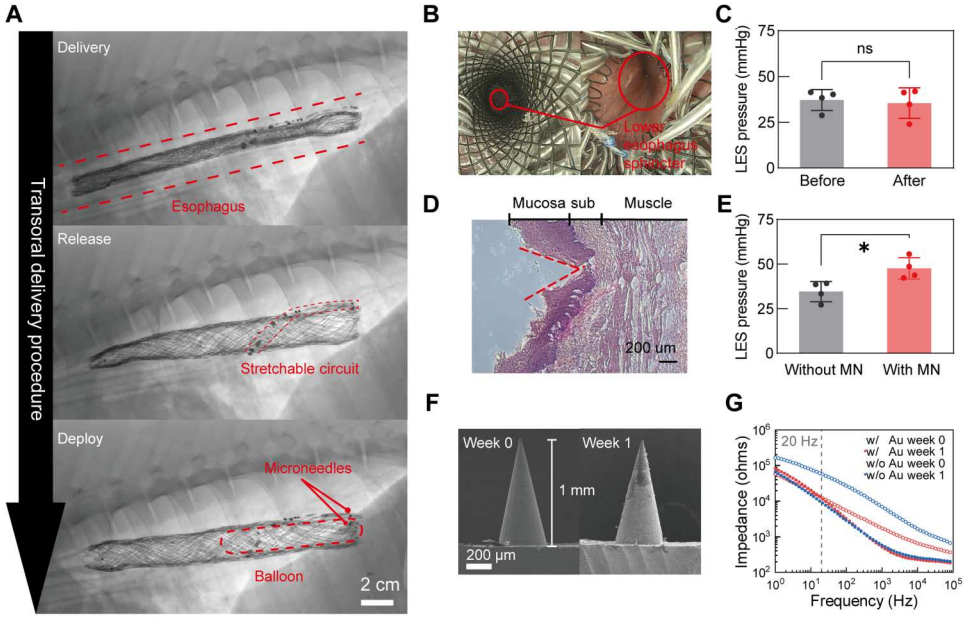

Fig. 3. Transoral delivery of E-Stent. (**A**) X-ray images showing the transoral delivery procedure in vivo in a pig's esophagus. (**B**) Endoscopic view of E-Stent deployed in vivo inside the esophagus with closed LES. (**C**) Average LES pressure before and after E-Stent deployment. Paired *t* test shows no significant pressure changes before and after E-Stent deployment. Mean ± SD for $N = 4$ pigs. ns, not significant. ($P = 0.4709$). (**D**) In vivo histology analysis of MNs penetrating across esophageal mucosa without perforation. (**E**) Average LES pressure during stimulations of E-Stent without and with MNs. Paired *t* test shows that E-Stent with MN effectively increases LES pressure compared with groups without MN. Mean ± SD for $N = 4$ pigs. *$P = 0.0408$. (**F**) SEM images of MNs with 200-nm Au coatings before and after 1-week immersion in SGFs (pH 1.5). (**G**) Impedance spectra of MNs with and without Au coatings before and after 1-week immersion in SGFs (pH 1.5).

In vivo evaluation of the wireless stimulation of LES by E-Stent

To evaluate the efficacy of electrical stimulation of LES applied by the wireless-powered E-Stent, we performed in vivo studies with four pigs for its similar anatomical structure of the GI tract with human (*45*). Figure 4A shows an illustration of the test setup and working principle of the in vivo study. An anesthetized pig lies in the power transmitter (fig. S22) with a cylindrical workspace (40 cm in diameter and 25 cm in length). The uniform magnetic field generated within the workspace (fig. S5) allows wireless power transfer to E-Stent located in the deep tissue of large animals. Movie S7 demonstrates the wirelessly powered E-Stent with LED flashing at the programmed frequency and pulse width in vivo inside a pig's esophagus.

The efficacy of electrical stimulation of E-Stent is evaluated by the LES pressure measured by a water-perfused manometry catheter (Mui Scientific) covered with a dent sleeve, which is placed at the LES zone (fig. S23 and Materials and Methods). Figure 4B shows the profile of LES pressure measured before (Base, 5 min), during (Stim, 20 min), and after electrical stimulations (Post, 20 min). One-

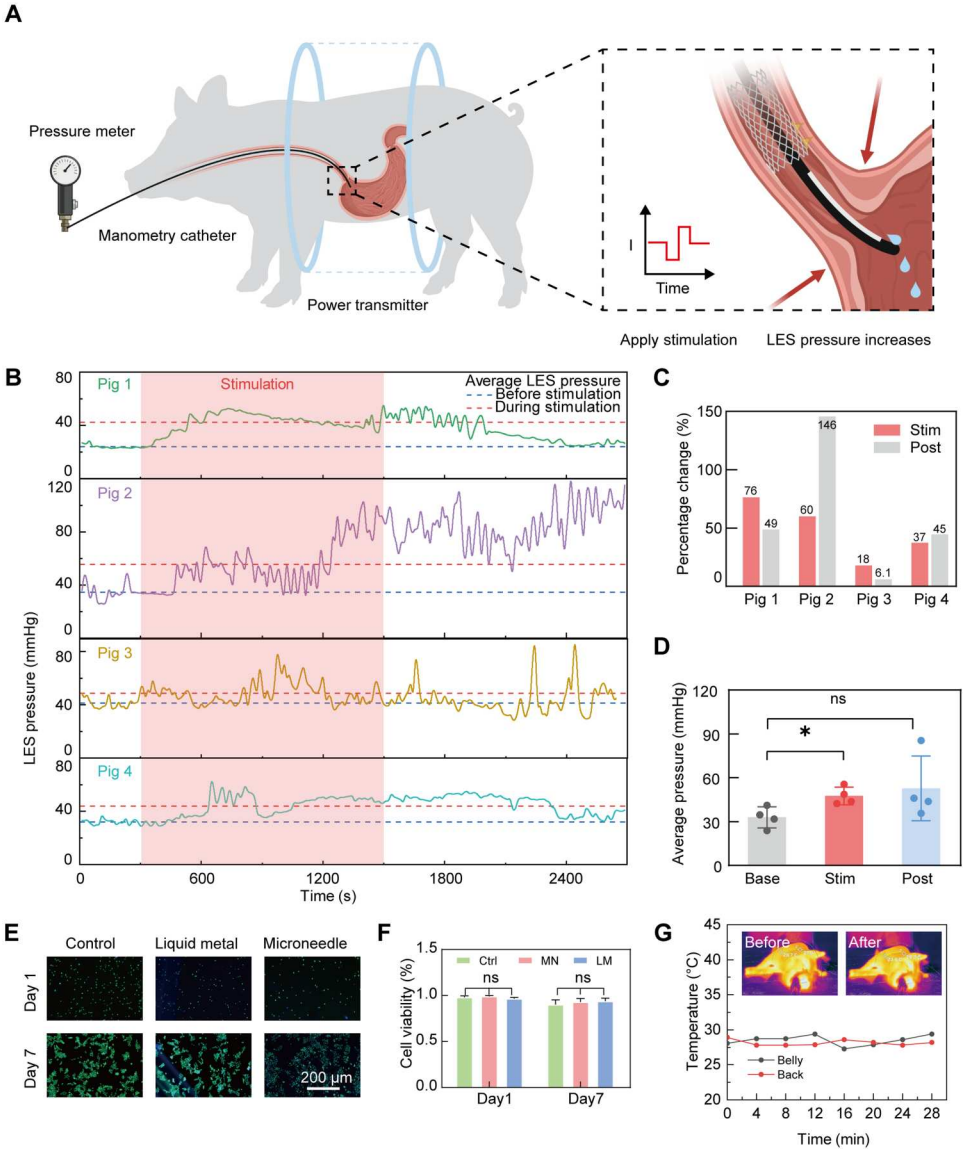

Fig. 4. In vivo electrical stimulation of the LES in pigs. (**A**) Schematic illustration showing the experimental setup for the in vivo electrical stimulation. A pig lies in the power transmitter. A water-perfused catheter that measures the pressure of LES is inserted through the esophagus. After applying electrical stimulations, the LES pressure increases. (**B**) The pressure profile of the LES before (Base), during (Stim), and after (Post) stimulations ($N = 4$). (**C**) Percentage increment of average LES pressure of four pigs during (Stim) and after (Post) stimulation sessions. (**D**) Average LES pressure during Base, Stim, and Post sessions. Paired t test shows that electrical stimulations significantly increase LES pressure compared with baseline. Mean ± SD for $N = 4$ pigs. $^*P = 0.0172$. ns, not significant. ($P = 0.1584$). (**E**) Fluorescence images of live (green)/dead (red) human esophagus epithelium cells (Het-1A) for silicone tubes with LM and MNs with Au coating. (**F**) Cell viability of Het-1A cells of control (Ctrl), MNs with Au coating, and silicone tubes with LM for 1 week. (**G**) Temperature changes of pig skin during wireless power transfer. Infrared camera images before and after stimulations (inset).

way analysis of variance (ANOVA) test is performed for each pig (fig. S24), and the results show that significant pressure increases after stimulations for all pigs. Compared with the baseline (average pressure before stimulations), average LES pressure during stimulation sessions increases from 18 to 76% in four pigs. During 20-min rest sessions, the average pressure still maintains higher than baseline from 6.1 to 146% (Fig. 4C). Moreover, the average LES pressures for each pig at different stages are then calculated for statistical analysis. Paired *t* test shows a statistically significant increase in LES pressure during stimulations but no significant pressure change after 20-min rest (Fig. 4D). These experiments demonstrated that, in our animal cohort, the wireless-powered E-Stent can provide continuous electrical stimulation to reinforce LES pressures.

Considering potential human translation, safety of the proposed device must be investigated. We perform biocompatibility test of used materials (MNs and silicone-covered LM) with human esophagus epithelial cells (Het-1A). Figure 4 (E and F) shows that Au-coated MNs and LM-filled silicone tube do not affect cell proliferation and viability, indicating no cytotoxicity and great biocompatibility of our device. To further evaluate the safety of the wireless power transfer system, specific absorption rate (SAR) is simulated by finite element analysis (see details in Materials and Methods). A simplified body trunk comprising skin, fat, and muscle is placed inside the power transmitter with a driving current of 2 A at the working frequency of 220 kHz (fig. S25). The SAR profile shows that the dissipated power is focused on the skin near the transmitter coil with a peak exposure value of 0.113 W/kg, which is far below the threshold of 0.4 W/kg (*46*). Moreover, heating effect is quantitatively evaluated by monitoring the skin temperature of a pig using an infrared camera during the operation of power transmitter. The minimal temperature change during wireless power transfer validates the SAR safety (Fig. 4G). The in vivo feasibility study in the pig models demonstrates the efficacy and safety of E-Stent and its potential translation in adult patients.

DISCUSSION

We design the wireless, battery-free E-Stent integrated with stretchable electronic circuits and demonstrate its feasibility in the transoral delivery procedure and continuous electrical stimulation in adult pig models. E-Stent is wirelessly powered on the basis of magnetic resonant coupling and thus eliminates the need for bulky batteries in conventional implantable pulse generators. The superelastic feature of the nitinol stent and elastic coil allows E-Stent to undergo large deformations without damage, enabling the delivery procedure through the esophagus. The transoral method minimizes the potential risk of open surgery for the implantation or removal of conventional stimulators. Continuous electrical stimulation in swine significantly increases the pressure of LES, which suggests that intermittent electrical stimulation could be a promising solution for effective symptom control and prevention of acid reflux (*47*).

Considering potential human translation, a wearable power transmitter with a portable control module and power supply would be the critical parts for this system. We summarize a strategy (fig. S26) to design wearable power transmitters to accommodate different patients' body sizes. We demonstrate the design strategy by developing two wearable power transmitters with different sizes for the slim volunteer (height: 177 cm, weight: 60 kg; fig. S27A) and the one with mild obesity (height: 175 cm, weight: 87 kg; fig. S27E) correlating to GERD (*48*). We also did the simulation and found out that these two transmitters can generate relatively uniform magnetic fields at the surrounded space (with a range of 40 cm), which is essential to power our E-Stent through deep tissue (fig. S27, B, C, F, and G).

We also use a transparent human model to better demonstrate the wearable power transmitter on patients and its capability of powering our E-Stent located inside the human body. As shown in movie S1 and fig. S1, the human model wore the power transmitter, which is controlled and powered by a portable control box and a rechargeable lithium battery (output voltage: 3.7 V, capacity: 20 Ah, weight: 331.5 g) (fig. S28). In this demonstration, we set the driving current as 0.5 A to power the transmitter coils, which can power E-Stent for over 24 hours with a single charging of lithium battery. Although we used an adjustable capacitor with a large size for the prototype of portable control box in this demonstration (fig. S28B), it is feasible to make a more compact and user-friendly version of control box by replacing the large adjustable capacitor with a series of onboard capacitors.

In addition, there is a gap from the proof-of-concept product to a clinical product. Despite the low cost of laboratory-made E-Stent (table S3), the low yield is a major problem in stretchable bioelectronics. Fabrication methods should be improved to leverage the successful rate and throughput. Although the laser-assisted fabrication shows great potential for batch fabrication, integrating soft electronics on 3D objects with transformable structures, like stents and balloon catheters, still remains a challenge. Roll-to-roll printing techniques and pop-up MNs would be promising solutions (*25*, *49*–*51*). Additional engineering functions should be integrated with the current system for practical usage. For example, digital-to-analog converters can be used to control the amplitudes of stimulation currents, and wireless communication modules can be integrated to program stimulation parameters wirelessly.

Long-term viability of E-Stent should be evaluated in future studies. Although we have demonstrated the retention of E-Stent in ex vivo esophagus with artificial peristalsis movement (fig. S29), E-Stent still suffers from the potential migration due to the repeat contraction of the esophagus during swallowing. E-Stent can be repositioned by an endoscopic operation through the mouth with minimal invasiveness. Despite that various adhesive strategies have been proposed for wet conditions (*52*–*54*), chronic retention remains the major challenge for mucosa-interfaced electronics due to the rapid cellular turnover rate and slippery and dynamic in vivo environment (*55*). Physical adherence approaches such as hooked needles interfacing with epithelial cells that have lower turnover rates are another promising solution to enable month-long retention (*25*, *26*).

E-Stent allows access to the internal lumen and biofluids of the GI tract in a noninvasive method. In the future, integrating E-Stent with sensors, such as pressure sensors or biosensors (*56*), would provide a platform for the bi-direction interface capable of simultaneous diagnosis and treatment of GI disorders. Patient-specific pathophysiological assessments offer an opportunity for personalized closed-loop treatment (*23*, *57*). Other nonpharmacologic therapies could also be integrated with E-Stent. Wirelessly powered optical therapies, like photodynamic therapy (*36*) and optogenetics (*28*), are promising for noninvasive treatment. Specifically,

wirelessly powered phototherapy is efficacious in treating *Helicobacter pylori* infection (*58*), and optogenetics could regulate colonic motility (*59*).

MATERIALS AND METHODS

In vivo animal studies

Animal experiments in this study were carried out in accordance with the guidelines of the Animals Ordinance (Chapter 340), Department of Health, Hong Kong. All the procedures were approved by the Institutional Animal Care and Use Committee of the Hong Kong Science and Technology Parks Corporation and Animal Experimentation Ethics Committee of the Chinese University of Hong Kong. Four adult pigs (two male and two female) used in the experiment are food-restricted for 24 hours before the procedures. For anesthesia, the pig is first sedated by injecting with a mixture of atropine, xylazine, and ketamine. Then, anesthesia is maintained by 4% pentobarbitone. During the surgical procedures, a 1:1 mixture of 2% isoflurane to oxygen and nitrous oxide is inhaled at a rate of 5 liters/min.

Fabrication of the elastic coils

EGaIn is prepared by melting gallium and indium with a weight ratio of 3:1 at 180°C. The conductive and elastic coil is made by injecting the EGaIn alloy into a hollow silicone tube (with an outer diameter of 0.8 mm and an inner diameter of 0.3 mm). Then, the single-strand wire is braided along with the skeleton of a commercially available esophageal stent (MicroTech). Double-strand copper wires are inserted into both ends of the elastic coils, and the connection is encapsulated by epoxy to avoid the leakage of EGaIn.

Characterization of the elastic coils

The intrinsic parameters, including the inductance and the quality factor of the elastic coils, are measured by an LCR meter (IM3536, HIOKI). The open-circuit voltages of the elastic coils are measured with an oscilloscope (TBS 2104, Tektronix). When measuring the power, the elastic coils are connected to a resistor box. Voltages are recorded when the resistor is swept from 10 to 10,000 ohms. Corresponding power is calculated on the basis of Ohm′s law.

When measuring the voltage and power with angular misalignment, elastic coils are fixed by a series of 3D-printed supports (Pro2, Raise3D) with different angles with respect to the axis of the transmitter coil. When measuring the voltage and power under compression, elastic coils are compressed by acrylic tubes with different inner diameters. Voltages with different compressions are measured, and related power is calculated. For in vivo measurement, an elastic coil with an extra 1-m length is delivered inside the esophagus, while the output is extruded out of the pig′s mouth for the measurement. Inductance, voltage, and power are measured in the same way described above. S11 values of the elastic coils are measured with a portable vector analyzer (miniVNA PRO 1300).

Fabrication of the stretchable circuit

The stretchable substrates of PDMS elastomer (Sylgard 184 with a 10:1 base-to-curing agent ratio, Dow Corning) are cured on a glass substrate. A thin metal film of 20-nm Cr followed by 100-nm Au is deposited by E-beam evaporation (EB-600, IVS). Then, the PDMS substrate with Au coating was fully immersed in the EGaIn and 3 weight % (wt%) NaOH solution following with shaking the bulk EGaIn above the substrate for about 1 min for fully alloying between EGaIn and gold. Extra EGaIn was then removed by titling the substrate and cleaned by deionized water after EGaIn dropping. A 1064-nm fiber laser was used to pattern the circuit trace (Universal Laser System Ultra R5000, speed: 100%, power: 90%, repeated two times). Pins of electronics are also immersed in EGaIn with 3 wt% NaOH solution to deposit a thin layer of LM on the footprints. These pins are then cleaned by deionized water to wash away the NaOH solution, and extra water is dried by paper tissue. The native oxide layer of EGaIn will be fractured by gently placing the electrical components on the circuit traces. Last, entire circuits are encapsulated with PDMS.

Mechanical property characterization

An esophageal stent (NST01-221-20.120, MicroTech) with a length of 120 mm and a diameter of 20 mm is used for the compression test. The integrated E-Stents were compressed at the midpoint with a 12.7-mm-diameter flat head attachment by an extensometer (Mach) with a loading speed of 0.1 mm/s. Cyclical stretching and bending tests are performed with an Instron extensometer, and the cyclical twisting test is performed by a customized mechanical test system.

Characterizations of MN electrodes

Copper MNs with a length of 1 mm were purchased from Taizhou Microchip Pharmaceutical Technology Co. Ltd., China. SEM image was obtained using a JEOL JSM-7800F scanning electron microscope. For the acid stability test, a 200-nm layer of Au is deposited on the surface of the electrodes by e-beam evaporation. SGF is prepared by dissolving sodium chloride (2.0 g/liter) in HCl solution (pH 1.5). MNs are fully immersed in SGF for 1 week. After cleaning with deionized water and drying, electrochemical analysis was performed with a potentiostat (CHI630E, CH Instruments) using a three-electrode configuration in phosphate-buffered saline (pH 7.4). Impedance analysis uses an AC perturbation amplitude of 10 mV sweeping from 1 to 10^5 Hz.

Histology analysis

Histological analysis was performed to characterize the depth of penetration. After the esophageal tissues were fixed in 10% formalin solution (CITOTEST), dehydrated using a series of ethanol solutions, embedded in paraffin, and cut into sections at 5-μm thickness, the sections were deparaffinized and rehydrated for hematoxylin and eosin staining. Images were captured with a fluorescence microscope (Nikon Eclipse Ti) with bright light.

In vivo electrical stimulation

The in vivo electrical stimulation was conducted in adult pigs. Before electrical stimulation, the pig was anesthetized and placed inside the transmitter coil (fig. S22). After E-Stent was delivered through the esophagus above the gastroesophageal junction, continuous electrical stimulation was initiated by turning on the transmitter coil with a driving current of 2 A.

LES pressure measurement

The LES pressure was measured with a water-perfused manometry catheter (CE2OESOPH-SL-CLIN3, Mui Scientific). Water was circulated through the channel by a water pump with a constant flow

rate of 0.3 ml/min. The catheter was inserted through the LES with an endoscope (GIF-HQ190; Olympus). One channel was covered by a section of a sleeve with a length of 6 cm, which reflected the maximum pressure applied to the sleeve. Pressure was read out with a digital pressure meter and recorded every 12 s. Pressure was measured through in vivo experiments, including four sessions, 5-min baseline measurement before and after E-Stent deployment, and 20-min pressure profile during and after stimulations.

Electromagnetic simulation

The electromagnetic field distribution of the transmitter coil was simulated by finite element analysis (COMSOL Multiphysics 5.3a, COMSOL Inc.) The transmitter coil was a pair of solenoid coils fixed on a customized plastic cylinder. In addition, the coils were simplified as homogenized multiturn coils.

The SAR simulation was conducted (COMSOL Multiphysics 5.3a, COMSOL Inc.). The transmitting coils were fixed on a custom-designed plastic cylinder, powering a current of 2 A at a frequency of 220 kHz. The trunk was schematized as a multilayer column composed of inner muscle covered by fat and skin layers (fig. S25). The dielectric properties of tissues were taken from http://niremf.ifac.cnr.it/tissprop/.

Cell viability

Thirty thousand human esophageal epithelial cells (Het-1A, Beijing Zhongkezhijian Biotechnology) were seeded in the 3-cm plate and cocultured with MNs and LM separately. The MNs were glued to the side wall of the culture dish in advance, and the culture medium covered the entire MN. Silicone tubes filled with LM were exposed to the LM group, ensuring full contact between the LM and the cell culture environment. After 7 days of persistent coculture, cells were dyed with propidium iodide (PI), calcein acetoxymethyl (AM), and Hoechst for 10 min. Photographs were taken under a fluorescent microscope, and then cell viability was calculated by the ratio of live cells (AM^+ and PI^-) to the total cells ($Hoechst^+$).

Supplementary Materials

This PDF file includes:
Texts S1 and S2
Figs. S1 to S28
Tables S1 to S3
Legends for movies S1 to S7
Legends for data files S1 to S9

Other Supplementary Material for this manuscript includes the following:
Movies S1 to S7
Data files S1 to S9

View/request a protocol for this paper from *Bio-protocol*.

REFERENCES AND NOTES

1. J. Dent, H. B. El-Serag, M.-A. Wallander, S. Johansson, Epidemiology of gastro-oesophageal reflux disease: A systematic review. *Gut* **54**, 710–717 (2005).
2. J. C. Wu, Gastroesophageal reflux disease: An Asian perspective. *J. Gastroenterol. Hepatol.* **23**, 1785–1793 (2008).
3. J. Maret-Ouda, S. R. Markar, J. Lagergren, Gastroesophageal reflux disease: A review. *JAMA* **324**, 2536–2547 (2020).
4. N. Vakil, S. V. van Zanten, P. Kahrilas, J. Dent, R. Jones; Global Consensus Group, The Montreal definition and classification of gastroesophageal reflux disease: A global evidence-based consensus. *Am. J. Gastroenterol.* **101**, 1900–1920 (2006).
5. A. Kandulski, P. Malfertheiner, Gastroesophageal reflux disease—From reflux episodes to mucosal inflammation. *Nat. Rev. Gastroenterol. Hepatol.* **9**, 15–22 (2012).
6. N. J. Shaheen, J. E. Richter, Barrett's oesophagus. *Lancet* **373**, 850–861 (2009).
7. N. Shaheen, D. F. Ransohoff, Gastroesophageal reflux, Barrett esophagus, and esophageal cancer: Scientific review. *JAMA* **287**, 1972–1981 (2002).
8. A. P. Hungin, G. Rubin, H. O'Flanagan, Factors influencing compliance in long-term proton pump inhibitor therapy in general practice. *Br. J. Gen. Pract.* **49**, 463–464 (1999).
9. D. Sifrim, F. Zerbib, Diagnosis and management of patients with reflux symptoms refractory to proton pump inhibitors. *Gut* **61**, 1340–1354 (2012).
10. N. Vakil, M. Shaw, R. Kirby, Clinical effectiveness of laparoscopic fundoplication in a U.S. community. *Am. J. Med.* **114**, 1–5 (2003).
11. R. A. Ganz, J. H. Peters, S. Horgan, W. A. Bemelman, C. M. Dunst, S. A. Edmundowicz, J. C. Lipham, J. D. Luketich, W. S. Melvin, B. K. Oelschlager, S. C. Schlack-Haerer, C. D. Smith, C. C. Smith, D. Dunn, P. A. Taiganides, Esophageal sphincter device for gastroesophageal reflux disease. *N. Engl. J. Med.* **368**, 719–727 (2013).
12. L. Martin, M. Stavrou, F. el Madani, S. Gupta, PTU-195 six years of laparoscopic Nissen's fundoplication, was it worth it? An audit of 100 patients. *Gut* **61**, –A265 (2012).
13. L. Bonavina, T. DeMeester, P. Fockens, D. Dunn, G. Saino, D. Bona, J. Lipham, W. Bemelman, R. A. Ganz, Laparoscopic sphincter augmentation device eliminates reflux symptoms and normalizes esophageal acid exposure: One- and 2-year results of a feasibility trial. *Ann. Surg.* **252**, 857–862 (2010).
14. C. Avci, Complication in laparoscopic GERD: A guide to prevention and management, in *Complications in Laparoscopic Surgery* (Springer, 2016), pp. 37–57.
15. R. Fass, D. Sifrim, Management of heartburn not responding to proton pump inhibitors. *Gut* **58**, 295–309 (2009).
16. Y. R. Wang, D. T. Dempsey, J. E. Richter, Trends and perioperative outcomes of inpatient antireflux surgery in the United States, 1993–2006. *Dis. Esophagus* **24**, 215–223 (2011).
17. G. Triadafilopoulos, D. Azagury, How can we deal with the GERD treatment gap? *Ann. N. Y. Acad. Sci.* **1381**, 14–20 (2016).
18. S. E. Kim, E. Soffer, Electrical stimulation for gastroesophageal reflux disease: Current state of the art. *Clin. Exp. Gastroenterol.* **9**, 11–19 (2016).
19. I. Franks, Electrical stimulation of the lower esophageal sphincter to treat GERD. *Nat. Rev. Gastroenterol. Hepatol.* **9**, 190 (2012).
20. L. Rodriguez, P. Rodriguez, B. Gómez, J. C. Ayala, D. Oksenberg, A. Perez-Castilla, M. G. Netto, E. Soffer, M. D. Crowell, Long-term results of electrical stimulation of the lower esophageal sphincter for the treatment of gastroesophageal reflux disease. *Endoscopy* **45**, 595–604 (2013).
21. E. Soffer, Endostim implantation, in *Management of Gastroesophageal Reflux Disease* (Springer, 2020), pp. 183–192.
22. EndoStim Lower Esophageal Sphincter Stimulation Therapy, Patient Manual, Revision C; https://endostim.com/wp-content/uploads/2020/01/EndoStim-IDE-Patient-Manual.pdf.
23. K. B. Ramadi, S. S. Srinivasan, G. Traverso, Electroceuticals in the gastrointestinal tract. *Trends Pharmacol. Sci.* **41**, 960–976 (2020).
24. C. Steiger, A. Abramson, P. Nadeau, A. P. Chandrakasan, R. Langer, G. Traverso, Ingestible electronics for diagnostics and therapy. *Nat. Rev. Mater.* **4**, 83–98 (2019).
25. S. Babaee, Y. Shi, S. Abbasalizadeh, S. Tamang, K. Hess, J. E. Collins, K. Ishida, A. Lopes, M. Williams, M. Albaghdadi, A. M. Hayward, G. Traverso, Kirigami-inspired stents for sustained local delivery of therapeutics. *Nat. Mater.* **20**, 1085–1092 (2021).
26. A. Abramson, D. Dellal, Y. L. Kong, J. Zhou, Y. Gao, J. Collins, S. Tamang, J. Wainer, R. M. Manus, A. Hayward, M. R. Frederiksen, J. J. Water, B. Jensen, N. Roxhed, R. Langer, G. Traverso, Ingestible transiently anchoring electronics for microstimulation and conductive signaling. *Sci. Adv.* **6**, eaaz0127 (2020).
27. B. Wang, K. F. Chan, K. Yuan, Q. Wang, X. Xia, L. Yang, H. Ko, Y.-X. J. Wang, J. J. Y. Sung, P. W. Y. Chiu, L. Zhang, Endoscopy-assisted magnetic navigation of biohybrid soft microrobots with rapid endoluminal delivery and imaging. *Sci. Robot.* **6**, eabd2813 (2021).
28. S. M. Won, L. Cai, P. Gutruf, J. A. Rogers, Wireless and battery-free technologies for neuroengineering. *Nat.Biomed. Eng.*, 10.1038/s41551-021-00683-3 (2021).
29. J. C. Chen, P. Kan, Z. Yu, F. Alrashdan, R. Garcia, A. Singer, C. S. E. Lai, B. Avants, S. Crosby, Z. Li, B. Wang, M. M. Felicella, A. Robledo, A. V. Peterchev, S. M. Goetz, J. D. Hartgerink, S. A. Sheth, K. Yang, J. T. Robinson, A wireless millimetric magnetoelectric implant for the endovascular stimulation of peripheral nerves. *Nat. Biomed. Eng.* **6**, 706–716 (2022).
30. M. Silverå Ejneby, M. Jakešová, J. J. Ferrero, L. Migliaccio, I. Sahalianov, Z. Zhao, M. Berggren, D. Khodagholy, V. Đerek, J. N. Gelinas, E. D. Głowacki, Chronic electrical stimulation of peripheral nerves via deep-red light transduced by an implanted organic photocapacitor. *Nat. Biomed. Eng.* **6**, 741–753 (2022).

31. D. R. Agrawal, Y. Tanabe, D. Weng, A. Ma, S. Hsu, S.-Y. Liao, Z. Zhen, Z.-Y. Zhu, C. Sun, Z. Dong, F. Yang, H. F. Tse, A. S. Y. Poon, J. S. Ho, Conformal phased surfaces for wireless powering of bioelectronic microdevices. *Nat.Biomed. Eng.* **1**, 0043 (2017).
32. D. K. Piech, B. C. Johnson, K. Shen, M. M. Ghanbari, K. Y. Li, R. M. Neely, J. E. Kay, J. M. Carmena, M. M. Maharbiz, R. Muller, A wireless millimetre-scale implantable neural stimulator with ultrasonically powered bidirectional communication. *Nat.Biomed. Eng.* **4**, 207–222 (2020).
33. Z. Jia, G. Yan, Y. Shi, B. Zhu, A wireless power transmission system for an active capsule endoscope for colon inspection. *J. Med. Eng. Technol.* **36**, 235–241 (2012).
34. Z. Ma, Q. Huang, Q. Xu, Q. Zhuang, X. Zhao, Y. Yang, H. Qiu, Z. Yang, C. Wang, Y. Chai, Z. Zheng, Permeable superelastic liquid-metal fibre mat enables biocompatible and monolithic stretchable electronics. *Nat. Mater.* **20**, 859–868 (2021).
35. Y. Lu, Q. Hu, Y. Lin, D. B. Pacardo, C. Wang, W. Sun, F. S. Ligler, M. D. Dickey, Z. Gu, Transformable liquid-metal nanomedicine. *Nat. Commun.* **6**, 10066 (2015).
36. Y. Lee, D. H. Kim, Wireless metronomic photodynamic therapy. *Nat.Biomed. Eng.* **3**, 5–6 (2019).
37. K. Nan, S. Babaee, W. W. Chan, J. L. P. Kuosmanen, V. R. Feig, Y. Luo, S. S. Srinivasan, C. M. Patterson, A. M. Jebran, G. Traverso, Low-cost gastrointestinal manometry via silicone–liquid-metal pressure transducers resembling a quipu. *Nat. Biomed. Eng.* **6**, 1092–1104 (2022).
38. K. Yamagishi, W. Zhou, T. Ching, S. Y. Huang, M. Hashimoto, Ultra-deformable and tissue-adhesive liquid metal antennas with high wireless powering efficiency. *Adv. Mater.* **33**, 2008062 (2021).
39. C. Pan, K. Kumar, J. Li, E. J. Markvicka, P. R. Herman, C. Majidi, Visually imperceptible liquid-metal circuits for transparent, stretchable electronics with direct laser writing. *Adv. Mater.* **30**, 1706937 (2018).
40. I. V. Lam, Analysis of Improved Howland Current Pump Configurations (Application Report No. SBOA437A) (2023). Retrieved from Texas Instruments website: https://www.ti.com/lit/an/sboa437a/sboa437a.pdf?ts=1677162555260.
41. M. F. Ferhatoglu, T. Kıvılcım, Anatomy of Esophagus, in Esophageal Abnormalities. (Chai, 2017). doi: 10.5772/intechopen.69583.
42. A. M. Bellinger, M. Jafari, T. M. Grant, S. Zhang, H. C. Slater, E. A. Wenger, S. Mo, Y.-A. L. Lee, H. Mazdiyasni, L. Kogan, R. Barman, C. Cleveland, L. Booth, T. Bensel, D. Minahan, H. M. Hurowitz, T. Tai, J. Daily, B. Nikolic, L. Wood, P. A. Eckhoff, R. Langer, G. Traverso, Oral, ultra–long-lasting drug delivery: Application toward malaria elimination goals. *Sci. Transl. Med.* **8**, 365ra157 (2016).
43. C. P. Sanmiguel, M. Hagiike, M. P. Mintchev, R. D. Cruz, E. H. Phillips, S. A. Cunneen, J. L. Conklin, E. E. Soffer, Effect of electrical stimulation of the LES on LES pressure in a canine model. *Am. J. Physiol. Gastrointest. Liver Physiol.* **295**, G389–G394 (2008).
44. A. Hirsch, H. O. Michaud, A. P. Gerratt, S. de Mulatier, S. P. Lacour, Intrinsically stretchable biphasic (solid–liquid) thin metal films. *Adv. Mater.* **28**, 4507–4512 (2016).
45. L. Rodriguez, P. Rodríguez, M. G. Neto, J. C. Ayala, J. Saba, D. Berel, J. Conklin, E. Soffer, Short-term electrical stimulation of the lower esophageal sphincter increases sphincter pressure in patients with gastroesophageal reflux disease. *Neurogastroenterol. Motil.* **24**, 446–450 (2012).
46. International Commission on Non-Ionizing Radiation Protection (ICNIRP), Guidelines for limiting exposure to time-varying electric, magnetic, and electromagnetic fields (up to 300 GHz). *Health Phys.* **74**, 494–522 (1998).
47. L. Rodríguez, P. Rodriguez, B. Gómez, J. C. Ayala, D. Oxenberg, A. Perez-Castilla, M. G. Netto, E. Soffer, W. J. Boscardin, M. D. Crowell, Two-year results of intermittent electrical stimulation of the lower esophageal sphincter treatment of gastroesophageal reflux disease. *Surgery* **157**, 556–567 (2015).
48. S. Emerenziani, M. P. Rescio, M. P. L. Guarino, M. Cicala, Gastro-esophageal reflux disease and obesity, where is the link? *World J. Gastroenterol.* **19**, 6536–6539 (2013).
49. L. Jin, A. E. Forte, B. Deng, A. Rafsanjani, K. Bertoldi, Kirigami-inspired inflatables with programmable shapes. *Adv. Mater.* **32**, 2001863 (2020).
50. J. E. Park, H. S. Kang, M. Koo, C. Park, Autonomous surface reconciliation of a liquid-metal conductor micropatterned on a deformable hydrogel. *Adv. Mater.* **32**, 2002178 (2020).
51. Y. Gu, C. Wang, N. Kim, J. Zhang, T. M. Wang, J. Stowe, R. Nasiri, J. Li, D. Zhang, A. Yang, L. H.-H. Hsu, X. Dai, J. Mu, Z. Liu, M. Lin, W. Li, C. Wang, H. Gong, Y. Chen, Y. Lei, H. Hu, Y. Li, L. Zhang, Z. Huang, X. Zhang, S. Ahadian, P. Banik, L. Zhang, X. Jiang, P. J. Burke, A. Khademhosseini, A. D. McCulloch, S. Xu, Three-dimensional transistor arrays for intra- and inter-cellular recording. *Nat. Nanotechnol.* **17**, 292–300 (2022).
52. S. Baik, D. W. Kim, Y. Park, T.-J. Lee, S. Ho Bhang, C. Pang, A wet-tolerant adhesive patch inspired by protuberances in suction cups of octopi. *Nature* **546**, 396–400 (2017).
53. H. Yuk, C. E. Varela, C. S. Nabzdyk, X. Mao, R. F. Padera, E. T. Roche, X. Zhao, Dry double-sided tape for adhesion of wet tissues and devices. *Nature* **575**, 169–174 (2019).
54. Q. Yang, T. Wei, R. T. Yin, M. Wu, Y. Xu, J. Koo, Y. S. Choi, Z. Xie, S. W. Chen, I. Kandela, S. Yao, Y. Deng, R. Avila, T.-L. Liu, W. Bai, Y. Yang, M. Han, Q. Zhang, C. R. Haney, K. Benjamin Lee, K. Aras, T. Wang, M.-H. Seo, H. Luan, S. M. Lee, A. Brikha, N. Ghoreishi-Haack, L. Tran, I. Stepien, F. Aird, E. A. Waters, X. Yu, A. Banks, G. D. Trachiotis, J. M. Torkelson, Y. Huang, Y. Kozorovitskiy, I. R. Efimov, J. A. Rogers, Photocurable bioresorbable adhesives as functional interfaces between flexible bioelectronic devices and soft biological tissues. *Nat. Mater.* **20**, 1559–1570 (2021).
55. K. Nan, V. R. Feig, B. Ying, J. G. Howarth, Z. Kang, Y. Yang, G. Traverso, Mucosa-interfacing electronics. *Nat. Rev. Mater.* **7**, 908–925 (2022).
56. J. Li, Y. Liu, L. Yuan, B. Zhang, E. S. Bishop, K. Wang, J. Tang, Y.-Q. Zheng, W. Xu, S. Niu, L. Beker, T. L. Li, G. Chen, M. Diyaolu, A.-L. Thomas, V. Mottini, J. B.-H. Tok, J. C. Y. Dunn, B. Cui, S. P. Paşca, Y. Cui, A. Habtezion, X. Chen, Z. Bao, A tissue-like neurotransmitter sensor for the brain and gut. *Nature* **606**, 94–101 (2022).
57. Y. S. Choi, H. Jeong, R. T. Yin, R. Avila, A. Pfenniger, J. Yoo, J. Y. Lee, A. Tzavelis, Y. J. Lee, S. W. Chen, H. S. Knight, S. Kim, H.-Y. Ahn, G. Wickerson, A. Vázquez-Guardado, E. Higbee-Dempsey, B. A. Russo, M. A. Napolitano, T. J. Holleran, L. A. Razzak, A. N. Miniovich, G. Lee, B. Geist, B. Kim, S. Han, J. A. Brennan, K. Aras, S. S. Kwak, J. Kim, E. A. Waters, X. Yang, A. Burrell, K. San Chun, C. Liu, C. Wu, A. Y. Rwei, A. N. Spann, A. Banks, D. Johnson, Z. J. Zhang, C. R. Haney, S. H. Jin, A. V. Sahakian, Y. Huang, G. D. Trachiotis, B. P. Knight, R. K. Arora, I. R. Efimov, J. A. Rogers, A transient, closed-loop network of wireless, body-integrated devices for autonomous electrotherapy. *Science* **376**, 1006–1012 (2022).
58. G. Tortora, B. Orsini, P. Pecile, A. Menciassi, F. Fusi, G. Romano, An ingestible capsule for the photodynamic therapy of *Helicobacter pylori* infection. *IEEE/ASME Trans. Mechatron.* **21**, 1935–1942 (2016).
59. T. J. Hibberd, J. Feng, J. Luo, P. Yang, V. K. Samineni, R. W. Gereau IV, N. Kelley, H. Hu, N. J. Spencer, Optogenetic induction of colonic motility in mice. *Gastroenterology* **155**, 514–528.e6 (2018).

Acknowledgments: We thank T. Lam and K. Lai for performing x-ray fluoroscope imaging. Parts of Figs. 1, 3, and 4 were created with Biorender.com. **Funding:** The research work is financially supported by the Hong Kong RGC Research Fellow Scheme (RFS) with project no. RFS2122-4S03, the Croucher Foundation Grant with reference no. CAS20403, the ITF project with project no. ITS/440/17FP funded by the HKSAR Innovation and Technology Commission (ITC), and the CUHK internal grants. The authors also thank the support from Multi-Scale Medical Robotics Centre (MRC), InnoHK, at the Hong Kong Science Park, and the SIAT-CUHK Joint Laboratory of Robotics and Intelligent Systems. **Author contributions:** Conceptualization: C.Z., C.P., K.F.C., and L.Z. Methodology: C.Z., C.P., K.F.C., J.G., Z.Y., K.K.C.L., D.J., B.H., N.X., X.W., and S.J. Investigation: C.Z., C.P., K.F.C., Z.Y., Y.W., N.X., Z.N., Z.Z., and Q.W. Visualization: C.Z., C.P., and Z.Y. Supervision: K.F.C., P.W.Y.C., and L.Z. Writing—original draft: C.Z. and C.P. Writing—review and editing: K.F.C. and L.Z. **Competing interests:** L.Z, P.W.Y.C., K.F.C, C.Z., and C.P. are inventors on a U.S. Provisional Patent (U.S. application no. 63/446,026) on the wireless powered electrical stimulation systems and related methods. The other authors declare that they have no competing interests. **Data and materials availability:** No data were excluded from analysis. All data needed to evaluate the conclusions in the paper are present in the paper and/or the Supplementary Materials.

Submitted 13 September 2022
Accepted 3 February 2023
Published 8 March 2023
10.1126/sciadv.ade8622